Geotechnical Aspects of Underground Construction in Soft Ground, Mair & Taylor (eds)
 ISBN 90 5410 856 8

Finite element simulation of shield tunnelling processes in soft ground

H.Akagi
Waseda University, Tokyo, Japan
K.Komiya
Chiba Institute of Technology, Japan

ABSTRACT: This paper introduces a numerical simulation procedure for use with the shield tunnelling problems and compares the simulation results with field measurements for soft clay ground. Shield machine advance is simulated numerically by adopting excavation elements and repetitively rearranging the three-dimensional finite element mesh used in the simulation. Deformation of soft clay ground and the pore water pressure behaviour as the shield machine advances under actual hydraulic jacking forces are modelled successfully by the new procedure. As an example, the application of this procedure to the twin shield tunnelling problem is described.

1 INTRODUCTION

Over the last three decades, shield tunnelling has become one of the most powerful procedures used in the construction of urban tunnel structures. In urban areas, it is essential to protect pre-existing structures and underground conduits from damage during shield tunnelling. In order to accomplish this, it is necessary to predict the influence of tunnelling on neighbouring structures. Predictions of ground stress and deformation behaviour during shield tunnelling have in recent years been carried out by numerical analysis based on the finite element method.

Further, where twin shield tunnels are constructed, a second tunnel is often excavated in parallel with a pre-existing first tunnel. The clearance between parallel tunnels has been reduced below 0.5·D (D: Diameter of tunnel)(Horichi et al. 1990). In this situation, it is essential to evaluate the earth pressures acting on the tunnels for better prediction.

The current design practice of a shield tunnel takes the effect of pre-existing structures by varying the magnitude and distribution of the earth pressure based on the past field measurement records.

The numerical investigation of the interaction between two tunnels has been done in the past using finite element method or boundary element method(Itoh and Hisatake, 1981; Sugimoto et al. 1989; Miyakawa et al. 1995). By connecting the soil and tunnel elements together, the investigations examined the effects of initial stress, the geometrical arrangement of the two tunnels and the soil characteristics on the tunnel lining stress.

However, the finite element method generally used in shield tunnel design practice has been found to be too simple to model the actual processes of shield tunnelling. In particular, there have been many problems with finite element simulations of continuous excavation at the cutting face and of the tunnelling machine advancement processes.

This paper describes a new finite element technique, which takes the construction processes of shield tunnelling into account. The numerical analysis using this technique is first compared with the field measurement records of a single shield machine tunnelling in the soft ground to demonstrate the effectiveness of the technique. Finally, simulation of constructing twin shield tunnels is presented to show the changes in earth pressures acting on the tunnels during construction.

2 SOIL-WATER COUPLED FINITE ELEMENT MODELLING OF SHIELD TUNNELLING

Shield tunnelling causes extreme disturbances in the soil adjacent to the cutting head during excavation. Excavation elements are defined in front of the cutting head as a proposed method of rep-

resenting the area of ground disturbed by the excavation.

Figure 1 depicts the sequential behaviour of the finite element model as excavation is carried out by the cutting head and the tunnelling machine advances. The shaded elements in Fig.1 represent the excavation elements. Since these are extremely disturbed, their rigidity is small. Jacking forces act on the nodal points at the tail ends of shield machine at reference time t in Fig.1(a). The values of these forces were obtained from field measurements of hydraulic jack pressure. The excavation elements and other elements within the ground adjacent to the shield machine deform simultaneously under undrained or partly drained conditions due to these forces during time period dt, as shown in Fig.1(b). Since the rigidity of elements within the shield machine itself is much greater than those of other elements, deformation of the shield machine elements can be neglected.

After computing the displacements and stresses in the mesh arrangement shown in Fig.1(b), the finite element meshes are then rearranged as shown in Fig.1(c) with the correct stress and displacement fields to bring their geometric shape and size back to the original shown in Fig.1(a).

By repeating the procedure followed in Fig.1, the advancement of a shield machine and the associated changes in the stress-strain fields can be reproduced numerically in the finite element method.

Excavation and advancement cause large-magnitude deformations of the excavation elements in the direction of the force. Mesh rearrangement is necessary to avoid excessive deformation of the mesh. It is possible to introduce into the calculation factors to account for various practical execution procedures such as the clay slurry and water pressure acting on the cutting face in a slurry-type shield machine.

To simulate the pore water and soil interaction in the saturated ground, it is necessary to introduce into the analysis the coupling between deformation of the soil skeleton and movement of pore water. The finite element method can be used to incorporate this into the stress-deformation analysis of the saturated soil-water system. The effective stress change in a finite element is obtained from the diplacement vector at the nodal points constituting that element. When the model is rearranged, the correct effective stress field can be obtained from the displacement vector of the rearranged nodal points. The method used to obtain correct values of effective stress and pore water pressure in the rearranged finite element mesh within the ground is described as follows.

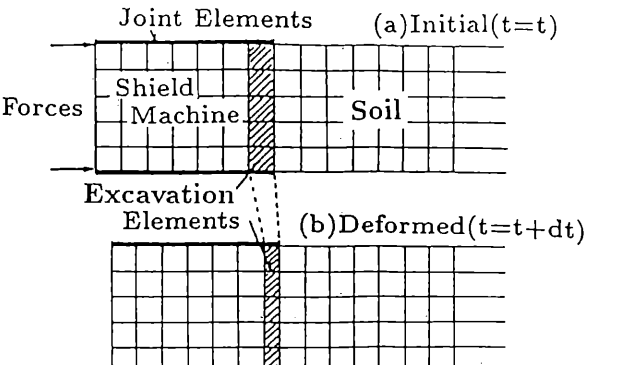

Fig.1 Advancement of the shield machine simulated by the excavation elements

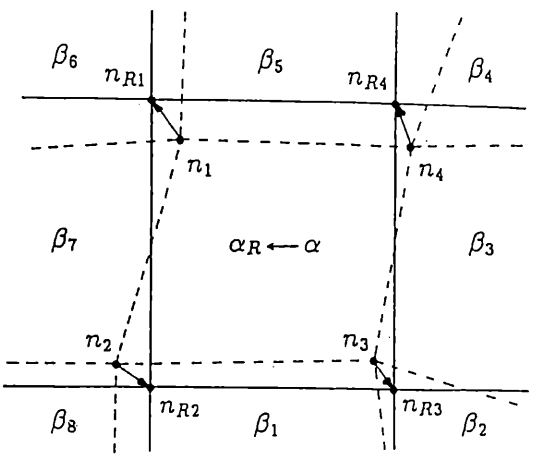

Fig.2 Rearrangement of finite element mesh

The broken lines in Fig.2 represent the deformed geometrical arrangement of the finite element mesh due to external forces, as shown in Fig.1(b), at reference time $t = t + dt$. The solid lines indicate the rearranged finite element mesh as shown in Fig.1(c) at the same reference time, $t = t + dt$. The initial values of effective stress and pore water pressure in the four-noded isotropic finite element α centered in the finite element mesh shown in Fig.2 are assumed to be $\{\sigma'_\alpha\}_t$ and p_α at reference time $t = t$. The effective stress change $\{\delta\sigma'_\alpha\}$ of element α associated with the nodal point displacement vector $\{\delta u_\alpha\}$, due to the external forces acting during time step dt as shown in Fig.1(a) and Fig.1(b),

is given by the following equation:

$$\{\delta\sigma'_\alpha\} = \int_{V_\alpha} [K_\alpha][B_\alpha]\{\delta u_\alpha\}dV \qquad (1)$$

where $[K_\alpha]$ is the element stiffness matrix of the soil skeleton, $[B_\alpha]$ is the strain-displacement matrix, and V_α is the volume of element α. Accordingly, the effective stress within this element $\{\sigma'_\alpha\}_{t+dt}$ at time $t = t + dt$ is described as follows.

$$\{\sigma'_\alpha\}_{t+dt} = \{\sigma'_\alpha\}_t + \{\delta\sigma'_\alpha\} \qquad (2)$$

This deformed finite element mesh, which is indicated by broken lines, is then rearranged into a regular rectangular finite element mesh represented by the solid lines in Fig.2. The displacement increment at a particular point within an isotropic finite element is easily calculated by substituting its local coordinate values for the shape function and using a displacement increment vector at the nodal points. The displacement increment vector $\{\delta u_{\alpha R}\}$ for the rearranged finite element nodal points, as represented by the solid-line crossing points in Fig.2, can be calculated as follows.

$$\{\delta u_{\alpha R}\} = \sum_{j=1}^{m} \{N_j^\alpha\}\{\delta u_{\alpha j}\} \qquad (3)$$

where $\{N_j^\alpha\}$ are the shape function values at a particular point in element α, $\{\delta u_{\alpha j}\}$ is the displacement increment vector at the nodal points, and m is the number of nodal points constituting a single finite element α. The effective stress increment $\{\delta\sigma'_{\alpha R}\}$ within the rearranged finite element α_R is represented as follows.

$$\{\delta\sigma'_{\alpha R}\} = \int_{V_\alpha} [K_\alpha][B_\alpha]\{\delta u_{\alpha R}\}dV \qquad (4)$$

The effective stress vector $\{\sigma'_{\alpha R}\}_{t+dt}$ within this rearranged finite element is obtained using the following equation.

$$\{\sigma'_{\alpha R}\}_{t+dt} = \{\sigma'_\alpha\}_{t+dt} + \{\delta\sigma'_{\alpha R}\} \qquad (5)$$

Since the effective stress principle is used in the analysis of soil-water coupling, the value of pore water pressure within the element must be corrected in order to satisfy the total stress equilibrium conditions. The corrected pore water pressure $p_{\alpha R}$ is obtained from the change in mean principal effective stress σ'_m within the finite element due to the rearrangement.

$$p_{\alpha R} = p_\alpha + \sigma'_m - \sigma'_{mR} \qquad (6)$$

where σ'_m is the mean principal effective stress of the element before rearrangement and σ'_{mR} is the value for the rearranged finite element mesh.

3 THREE-DIMENSONAL ELASTO-PLASTIC FINITE ELEMENT SIMULATION OF SHIELD TUNNELLING

During shield tunnelling, the position and movement of the shield machine is controlled by means of hydraulic jacks fitted behind it. Consequently, the orientation and direction of movement of the shield machine can vary in three directions; that is, the pitching and yawing motion of the shield machine can be complicated. Moreover, complex boundary conditions exist, particularly when shield tunnelling in urban areas, since the clearance between the tunnel and pre-existing underground structures is frequently very small. Accordingly, the three-dimensional effects of shield tunnelling on the neighbouring environment must be considered if rational design of shield tunnelling is to be achieved.

In this section, three-dimensional finite element analysis was carried out, taking account of the excavation procedures used in practical shield tunnel work and making use of the method described in the previous section. A practical example is adopted here: shield tunnelling with balanced earth pressure in the deep alluvial clay deposits found in the suburbs of Tokyo. The overburden depth is 32.8 m.

3.1 *Outline of analysis*

An ideal elastic constitutive equation, Hooke's law, was used for both shield machine elements and excavation elements. An elasto-plastic constitutive equation, the inviscid Sekiguchi-Ohta model, was used for the clay (Ohta and Sekiguchi,1979). Shield machine propulsion was numerically simulated by applying forces to the tail of the machine of a magnitude actually used to drive a shield machine. The three-dimensional finite element mesh is shown in Fig.3. The finite elements are the eight-noded isoparametric elements. The diameter of the shield machine is 3.737m and its length is 5.67m. The initial y-coordinate of the tail of the machine was arranged to be 2m in Fig.3 and the shield machine was driven forward in the positive y-axis direction. Excavation elements were placed in front of the shield machine; they had a thickness of 20cm. The air bubble pressure used

in the actual construction was applied within the excavation elements.

The input material parameters for clay were obtained on the basis of the standard geotechnical tests on undisturbed samples at various depths. The value of compression index, λ, for the clay was 0.320, the swelling index, κ, was 0.054, and the critical state parameter, M, was 1.05. The range of initial void ratio, e_0, for the clay was from 1.65 to 1.73 dependent on depth. Any needed parameters which could not be obtained from these tests were calculated using the method suggested by Iizuka(1988).

Since the excavation elements represent the volume disturbed by cutting and slurry mixing in front of the cutting face, the material properties of the excavation elements were difficult to obtain from experimental procedures. The excavation elements were assumed to be elastic with an elastic modulus as determined below. In this analysis, the excavated volume of soil, i.e. the amount by which the machine advances at each jacking, is governed by the volume change and shear distortion of the excavation elements. Thus the elastic modulus of the excavation elements was extremely important. A preliminary analysis was carried out by trial and error numerical simulations of excavation. An elastic modulus for each excavation element was obtained such that the shield advancement was equal to that in the field. The value of Young's modulus obtained in this preliminary analysis was 138.3(kN/m^2) and the Poisson's ratio ν of the excavation elements was equal to 0.100.

3.2 *Stress-deformation analysis of soft clay during shield tunnelling*

In this section, the stress-deformation behaviour of the soft clay during shield tunnelling was investigated based on a comparison of the results of a finite element analysis and the field measurements.

Vertical ground displacement was measured at the ground surface and within the ground. Pore water pressure changes were measured at a measurement point in the ground 1m above the crown of the shield machine, as illustrated in Fig.4.

Figure 5 is a comparison of the calculated results and measurement records for the case of vertical displacement at the ground surface and at the measurement point within the ground. The solid lines in Fig.5 represent calculated values and the broken lines are measurements. The horizontal axis of Fig.5 depicts elapsed time from the beginning of the numerical simulation. Although measurements in the ground indicate

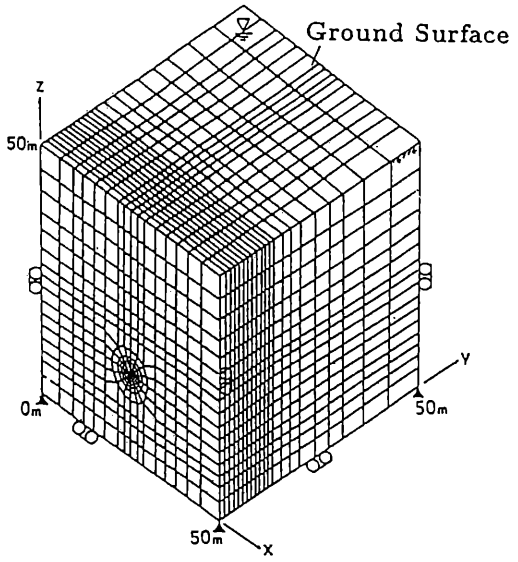

Fig.3 Finite element model used in the shield tunneling simulation

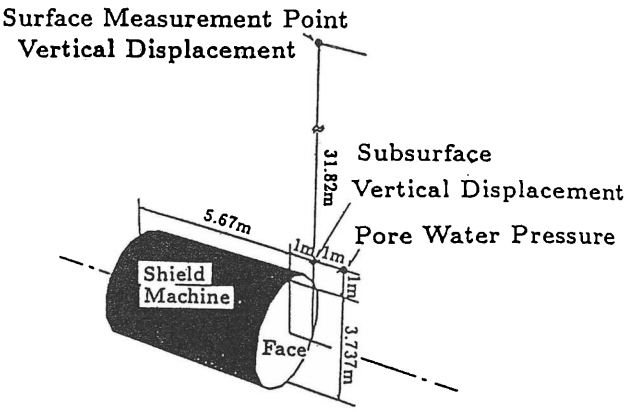

Fig.4 Location of in-situ measurement points for ground displacement and pore water pressure

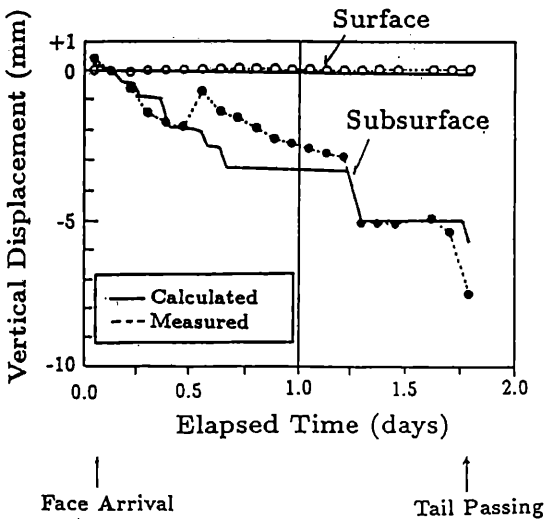

Fig.5 Variations in ground displacement against elapsed time

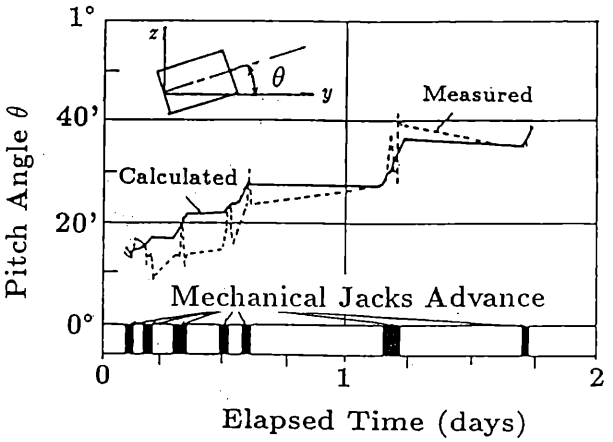

Fig.6 Variations in pitch angle against elapsed time

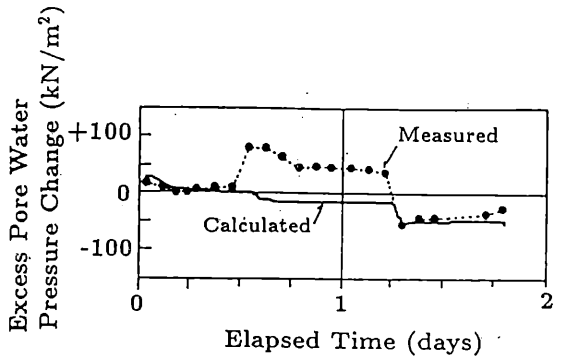

Fig.7 Variations in excess pore water pressure against elapsed time(Measeurement point)

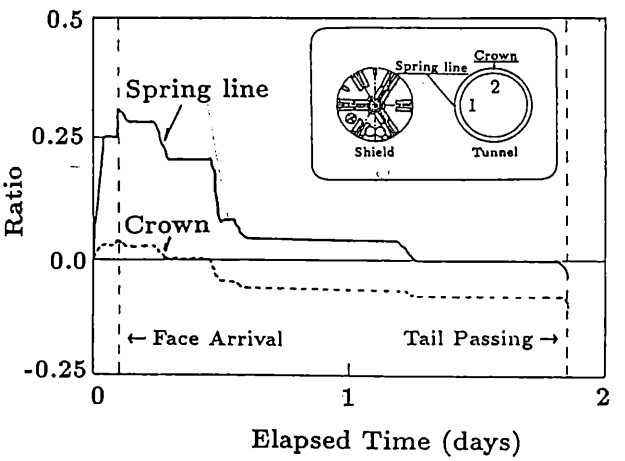

Fig.8 Time dependent variation in earth pressure

an unexpected large upheaval about 10 hours after the arrival of the shield machine face, the calculated and measured vertical displacements converge to almost the same values after the passage of the tail.

Figure 6 represents changes in the vertical tilt of the shield machine in terms of pitch angle, θ, versus the elapsed time. The value of θ is also defined in Fig.6. Since the shield machine was being driven upward, the pitch angle gradually increased as it advanced.

Figure 7 shows the variation in calculated and measured excess pore water pressure at the measurement point above the crown of the shield machine. Although a clear discrepancy exists between the measured and calculated values of excess pore pressure, the values ultimately settle to almost the same value.

These results demonstrate that vertical ground displacements and changes in excess pore water pressure during shield tunnelling are modelled numerically by the procedure proposed here. Most ground displacements and pore water pressure changes during shield tunnelling were shown to occur during advancement of the shield machine as its position and motion change.

4 APPLICATION TO TWIN SHIELD TUNNELLING

In this section, the new procedure was applied to the twin shield tunnel problem. The input parameters for ground conditions and the input data for the loads acting on the tail of the shield machine were the same as in the previous calculation. A pre-existing first tunnel of the same diameter(D=3.737m) as the second tunnel was assumed to be located at a distance of 0.5·D.

Figure 8 shows the time-dependent variation in earth pressure change ratio (=(pressure change)/(initial pressure)) acting on the first tunnel obtained at its springline and at the crown. Figure 9 gives the field measured earth pressure variations during excavation of the second shield tunnel under similar soil and geometrical boundary conditions (Horichi et al. 1990). A remarkable increase in earth pressure at the springline was observed in the field, and similar calculation results are obtained in Fig.8. A gradual decrease in earth pressure at the crown was measured and this is similar to the numerical calculation results shown in Fig.8. Table 1 compares the values of earth pressure obtained from field measurement records with the numerical simulation results. Since the overburden in the calculation case is much greater than that in the field, the absolute values of earth pressure in the finite element calculation are different. However, as a ratio, the values of earth pressure change (R and R') are almost the same as the field measurements.

Table 1. Comparison of earth pressure changes during twin shield tunnelling.

Legend	Measured at 1	Calculated at 1	Measured at 2	Calculated at 2
Initial Value p_0(kN/m^2)	220	520	180	490
Face Arrival p_1(kN/m^2)	300	675	165	520
Ratio $R = (p_1 - p_0)/p_0$	0.36	0.30	-0.08	0.06
Tail Passing p_2(kN/m^2)	205	484	150	435
Ratio $R' = (p_2 - p_0)/p_0$	-0.07	-0.07	-0.17	-0.11

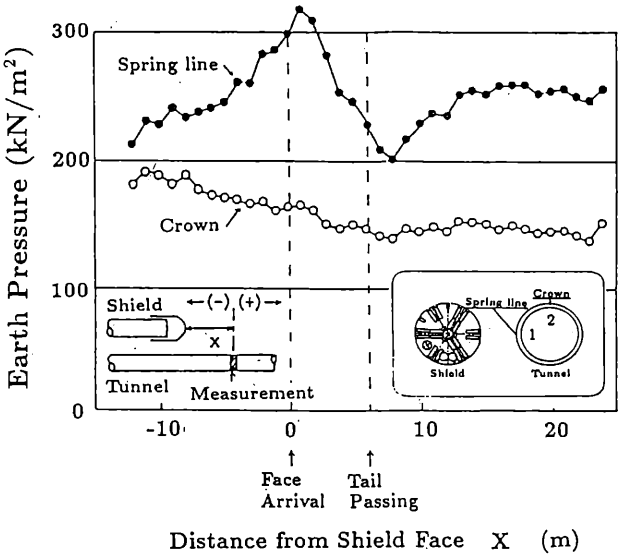

Fig.9 Field earth pressure variations

5 CONCLUSIONS

This paper introduces a new finite element technique to simulate construction processes of shield tunnelling. Excavation elements are proposed for the area in front of the cutting face. These represent the soil disturbed by cutting. A repetitive rearrangement of the finite element mesh is used in the calculation. A stress-deformation analysis of clay ground during shield tunnelling was carried out using this finite element method, taking into acount the actual construction process. The results were compared with field measurements. An example demonstrating the application of the proposed procedure to the twin shield tunnelling problem was shown. From the comparisons between the finite element calculation results and field measurements, it can be concluded that:

(1) advancement of the shield machine can be successfully simulated using the excavation elements and the repetitive mesh rearrangement proposed here.

(2) three-dimensional finite element simulation results for vertical ground displacement, excess pore water pressure changes, and postural changes of the shield machine correlate with field measurements.

(3) the changing earth pressure acting on the pre-existing tunnel during shield machine advance is successfully simulated by the proposed finite element simulation procedure.

ACKNOWLEDGEMENTS

The authors are grateful to Tokyo Electric Power Company, who provided the field measurement records used in this study. Thanks are also due to Kajima Corp. for their assistance in preparing the animation video, which illustrates the finite element simulation results.

REFERENCES

Horichi, N. et al. 1990, Evaluation of axial rigidity of shield tunnel considering the shear characteristics of interface materials, *Proc.JSCE*, No.415, 251-259 (in Japanese)

Iizuka, A. 1988, Study on the deformation and stability analyses of soft ground, Ph.D. Thesis, Kyoto University, 57-67 (in Japanese)

Itoh, T. and M.Hisatake 1981, Effects of second tunnel on the lining stress of pre-existing tunnel, *Proc.JSCE*, No.308, 77-84 (in Japanese)

Miyakawa, F. et al. 1995, Ground deformations during twin shield tunnelling and three dimensional F.E.M. analysis, *Proc.JSCE*, No.528, 17-30 (in Japanese)

Ohta, H. and H.Sekiguchi 1979, Constitutive equations considering anisotropy and stress reorientation in clay, *Proc.3rd ICNMG*, 475-484

Sugimoto, M. et al. 1989, Stability analysis of twin tunnel using elastic energy theory, *Proc.JSCE*, No.406, 185-194 (in Japanese)